ELSEVIER

Polymer 44 (2003) 2159–2168

polymer

www.elsevier.com/locate/polymer

Structural changes in non-isothermal crystallization process of melt-cooled polyoxymethylene[II] evolution of lamellar stacking structure derived from SAXS and WAXS data analysis

Hisakatsu Hama, Kohji Tashiro*

Department of Macromolecular Science, Graduate School of Science, Osaka University, 1-1 Machikaneyama-cho, Toyonaka, Osaka 560-0043, Japan

Received 29 November 2002; received in revised form 15 January 2003; accepted 16 January 2003

Abstract

Structural change occurring in the cooling process of polyoxymethylene from the molten state has been investigated by carrying out the temperature dependent measurements of small-angle X-ray scattering (SAXS) and wide-angle X-ray scattering (WAXS). In the SAXS experiment the generation of lamellar stacking structure with long period of ca. 14 nm was detected at first and then the new lamellae were inserted in between the already-existing lamellae to give the long period of 7 nm below 140 °C. The SAXS data were analyzed on the basis of lamellar insertion model by taking into account the second kind of paracrystalline disorder about the lamellar stacking mode. The thus obtained results were combined with the previously published infrared spectral data, and the structural change was deduced concretely. The generation of taut tie chains passing through the adjacent lamellae was proposed, which could reasonably explain the observation of infrared bands characteristic of extended-chain-crystal-like morphology.

Keywords: Polyoxymethylene; Crystallization; Small angle X-ray scattering

1. Introduction

Crystallization of polyoxymethylene (POM) has been investigated for a long time from various points of view [1–26]. But we have still many unsolved problems concerning the structural change in the crystallization process of this polymer. Even the lamellar stacking structure has not yet been definitely established, which could be solved on the basis of small-angle X-ray scattering (SAXS) data [1–3,22]. This information is important to discuss the evolution of stacked lamellar structure in the crystallization process.

As will be known in a later section, the SAXS of POM measured at room temperature consists of two peaks in most cases. The main peak is observed around $q_1 = 0.45\ \mathrm{nm}^{-1}$, where q is a scattering vector as defined later, and corresponds to the long period of ca. 14 nm. Another peak is observed at the position close to $2q_1$, though not necessarily exactly, and the peak height is usually much lower than the first main peak. But the relative height of these two peaks is dependent on the sample preparation condition and sometimes the intensity becomes comparable to that of the first peak. For the interpretation of these two peaks, there may be several possible ways. For example, the second peak is assumed as the second-order peak of the first one and therefore only one kind of stacked lamellar structure with the long period of ca. 14 nm is existent in the POM sample [see Fig. 1(a)]. The non-integer ratio of the positions between the first and second peaks has been considered to come from the effect of irregular lamellar stacking structure [27–37], as interpreted on the basis of a second-kind paracrystalline theory [28]. Another model is to assign the two SAXS peaks to the different structures with the different long periods, 14 and 7 nm. For example a low-molecular-weight component, which might be included in the sample, forms the stacked lamellae with 7 nm long period and coexists with the main lamellar structure of 14 nm long period independently [see Fig. 1(b)]. The third model is a lamella insertion model as shown in Fig. 1(c). The lamellae of 14 nm long period are formed at first and then the amorphous region sandwiched between the two

* Corresponding author. Tel./fax: +81-6-6850-5455.
E-mail address: ktashiro@chem.sci.osaka-u.ac.jp (K. Tashiro).

0032-3861/03/$ - see front matter © 2003 Elsevier Science Ltd. All rights reserved.
doi:10.1016/S0032-3861(03)00093-4

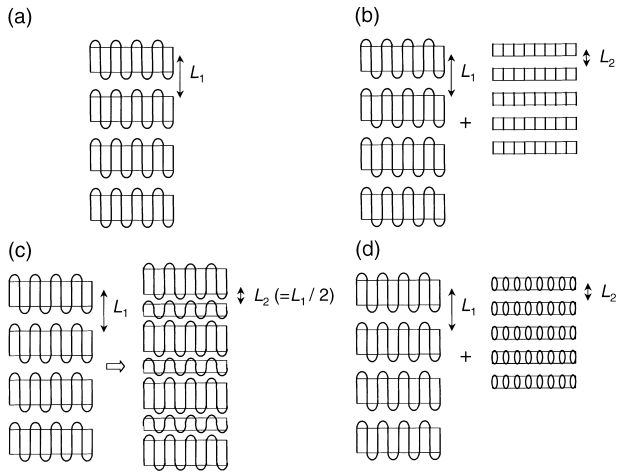

Fig. 1. Illustrated models of stacked lamellar structures. (a) 2-phase lamellar stacking model, (b) coexistence of the main lamellar stacking structure (L_1) and the stacked lamellae of linear low-molecular-weight compound (L_2), (c) insertion model of new lamellae in between the already-existing lamellar stacking structure, and (d) coexistence of the main lamellar stacking structure and the stacked lamellae of macrocyclic compounds. (It is noted here that the lamellae are stacked regularly in these models but they are more or less disordered in the actual samples as discussed in the text.)

adjacent lamellae changes to a new lamella to form the stacked lamellar structure of 7 nm long period. In the actual sample, the insertion of new lamella is not perfect but the lamellae of 14 and 7 nm long periods are coexistent to give the two SAXS peaks. Depending on the perfectness of insertion, the relative amount of these two structures is changed, reflecting on the relative intensity of the two SAXS peaks. Besides the stacking structure itself (e.g. the long period) may be disordered more or less in the actual sample. About the model shown in Fig. 1(d) the discussion will be made in a later section.

Which model is the most reasonable for the stacked lamellar structure of POM? This discussion was made extensively by Geil [22]. For example, according to his experiment, the long periods of stacked lamellar structure estimated from the electron microscopy (EM) and SAXS pattern were not coincident with each other: the long period obtained by EM was corresponded to the second SAXS peak of long period ca. 7 nm. The first SAXS peak with long period 14 nm was inconsistent with the EM data. Another problem is about the ratio of these two long periods, which is nearly equal to 2, although it changes depending on the preparation condition of samples. Geil pointed out a possibility of assignment of these two SAXS peaks to the different kinds of structure shown in Fig. 1 [22]. However, the similar observation was made for various kinds of polymers such as polyethylene [38–41], poly(ethylene terephthalate) [42], poly(aryletheretherketone) [43,44] and also for the blends of different types of polymers [45–49]: this ratio is about 2 commonly to these polymers. Why is this ratio common to these different kinds of polymers? Is there any inevitability essential to these semicrystalline polymers? To solve these problems about the stacked lamellar structure of POM is not only useful for the structural study of POM itself but also is very important as a general problem encountered in many crystalline polymers.

In the previous paper [50], we carried out the measurements of infrared spectra and SAXS/WAXS profiles in the cooling process from the melt of POM in order to clarify the structural changes occurring in the crystallization process. The infrared spectra of POM are quite useful for the study of crystallite morphology, folded chain crystal (FCC) and extended chain crystal (ECC) [51]. Depending on the difference in morphology, FCC or ECC, the infrared bands are observed at different wavenumber positions. The infrared data were combined with the SAXS data, and the crystallization of POM was described on the basis of a lamella insertion model, which was employed after the long discussion on the various possible models. The infrared bands intrinsic of FCC were found to behave in parallel with the stacked lamellae of 14 nm long period and the bands of ECC with the newly generated lamellar stacking structure of 7 nm long period. In this case, the ECC was not necessarily the separated crystallite but was interpreted as a bundle of taut tie chains passing through the several continuously stacked lamellae.

We told above that the lamella insertion model was employed as a finally chosen model after a long discussion. In the present paper, the details of the interpretation of SAXS data are described and the rational reasons for extracting a lamella insertion model will be listed up concretely. Then the structural evolution of stacked lamellae is presented on the basis of the SAXS and WAXS data combined with the previously-reported infrared data.

2. Experimental

2.1. Samples

The POM samples used here were the same with those in the previous paper [50]: in order to avoid thermal degradation as much as possible, a copolymer of trioxane with small content of ethylene oxide (ca. 2.2 wt%, Duracon M90, Polyplastics Co. Ltd., Japan) was used. The M_w was ca. 69,300 g/mol and M_w/M_n was ca. 2.3. As judged from the DSC, X-ray diffraction and IR spectral measurements, the crystallization behavior was essentially the same with that of the homopolymer sample (Delrin and Tenac).

2.2. Measurements

Temperature dependences of SAXS and WAXS were measured by using synchrotron radiation as an X-ray source at beam lines BL10C and BL15A, respectively, in Photon Factory of High-Energy Accelerator Research Organization in Tsukuba, Japan. The wavelength of incident X-ray beam

was 0.149 nm in both of BL10C and BL15A. The temperature was changed step by step from 205 °C to room temperature. The X-ray exposure was made for every 15 s in both the measurements. The detector was a PSPC (Position Sensitive Proportional Counter) for both of the measurements. In the analysis of SAXS data, correction of background and fluctuation of beam intensity was made and the scattering intensity $I(q)$ was transformed to $I(q)q^2$ for the correction of Lorentz factor, where q was a phonon vector defined as $q = (4\pi \sin\theta)/\lambda$ (λ = a wavelength of incident X-ray beam and 2θ = a scattering angle).

3. Results and discussion

3.1. Temperature dependence of SAXS profile

Fig. 2 shows the temperature dependence of SAXS profile measured in the slow cooling process of POM (M90) from the molten state. In the temperature region of 150 °C, the peak started to appear around $q = 0.35\ \mathrm{nm}^{-1}$ and increased in intensity. Careful observation of this peak profile told us that it was asymmetric and a shoulder was detected around $q = 0.6\ \mathrm{nm}^{-1}$, which could be assigned to the second-order component of the main peak. As the temperature decreased and approached to 140 °C, another peak appeared newly. The relative intensity of this new peak increased with decreasing temperature and became almost comparable at room temperature to that of the original peak at $q = 0.4\ \mathrm{nm}^{-1}$. The relative intensity of these two peaks is dependent on the cooling condition from the melt as shown later. In the case of comparatively fast cooling, the height of the second peak was low. But the very slow cooling gave higher intensity to the second peak.

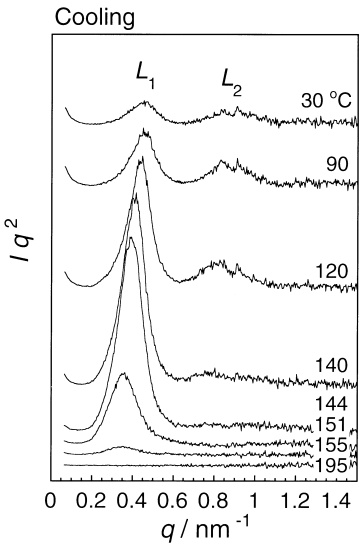

Fig. 2. Temperature dependence of SAXS profile of POM sample measured in cooling process from the melt.

3.2. Interpretation of the SAXS profile

In this section, the assignment of these two SAXS peaks, which are now named L_1 and L_2, respectively, will be made. As shown in Fig. 2, the temperature region to detect the L_2 peak is different from that of the L_1 peak. In other words, the temperature dependences of these two peaks are different from each other. The similar point can be said also about the time evolution of these two peaks. As will be reported in a separate paper, the molten POM sample was brought immediately to the temperature of crystallization and the time-resolved SAXS measurements were carried out. In this experiment, the L_1 peak was observed at first and then the L_2 peak appeared later, where the relative intensity of the L_1 peak became lower. In this way, the peaks L_1 and L_2 are considered to come from the different origins.

To what structures can we assign the peaks L_1 and L_2? As stated in the introductory section, the simplest consideration is to assume that the L_1 peak, the long period of which is ca. 14 nm at room temperature, reflects the stacked lamellar structure and the L_2 peak is assigned to the second-order peak of the main L_1 peak. But this assignment is inconsistent with the different temperature (and time) dependence between the L_1 and L_2 peaks. Another possibility is to assign the L_1 peak to the main lamellar stacking structure of ca. 14 nm long period and the L_2 peak to the other type of stacked lamellar structure with the long period 7 nm [see Fig. 1(b)]. At this moment, we need to remember the experimental result of infrared spectral measurement [50]. Judging from the good correspondency of the temperature (and time) dependence between the IR and SAXS data, the L_1 peak is connected with the FCC morphology and the L_2 peak with the ECC morphology. Therefore, as one possibility, the structure of the L_2 peak might be assumed to come from the low-molecular-weight chain component with fully-extended structure. Fig. 1(b) shows this model. That is, the POM sample is assumed to be a dual model consisting of the two kinds of the separated lamellar stacking structures. Since the observed long period (or long lattice spacing) of ECC lamella is ca. 7 nm and the helical pitch of POM chain is 0.193 nm per one monomeric unit [the fiber period of (9/5) helix is 1.739 nm [52,53] and therefore the pitch is equal to 1.739 nm/(9 monomer) = 0.193 nm], the number of monomeric units included in one short chain is about 36 (= 7 nm/0.193 nm). This corresponds to the molecular weight of 1100 g/mol. The actual POM sample used here has $M_w = 69,300$ g/mol [= (137,500 + 1100)/2] and $M_w/M_n = 2.3$. Since the relative intensity of SAXS is, roughly speaking, proportional to $N(\Delta\rho)^2$, where $\Delta\rho$ is an electron density difference and N is a number of lamellae, we need to consider the bimodal molecular weight distribution with two main peaks around $M = 137,500 \times$ g/mol and 1100 g/mol when we take the almost equal SAXS intensity of L_1 and L_2 peaks into account. Such a molecular weight distribution is inconsistent with that of the actual sample. Besides it is curious to employ a bimodal molecular

weight distribution when such an experimental observation is reminded that the relative intensity of L_1 and L_2 peaks was changed depending on the crystallization condition.

The POM sample shows the GPC profile with a small shoulder in the low-molecular-weight side [54,55]. This shoulder was assigned to the macrocyclic low-molecular-weight component, not a linear component, and the content was said to be less than 10% at most. That is, the third possibility is to assign the L_2 peak to the macrocyclic component which is contained in the POM sample prepared by a cationic polymerization reaction [54,55]. According to the concept of back-biting reaction [55], the macrocyclic compound is produced by combining the two ends of a folded chain loop and the length of macrocyclic ring should be almost equal to the lamellar thickness as seen in the illustration [see Figs. 1(d) and 3]. An aggregation of these macrocyclic compounds might give a long period of 7 nm. But this possibility is also difficult to employ when the content of these compounds is 10% at most, being inconsistent with the comparable SAXS intensity of the L_1 and L_2 peaks. The POM samples prepared by anionic polymerization reaction do not contain any such macrocyclic compounds, but they show essentially the same SAXS profiles with that of M90 used in this study, as shown in Fig. 4. The difference in relative intensity between L_1 and L_2 seems to come from the difference in the sample preparation condition and is not due to the difference in the content of such a macrocyclic low-molecular-weight component. As to the temperature dependence of the L_2 peak, low-molecular-weight compounds (either linear or macrocyclic) may show lower crystallization temperature than the main POM. Therefore it may be considered that the low-molecular-weight component crystallizes around 140 °C after the main component is crystallized at ca. 155 °C from the melt, reflecting on the observation of the

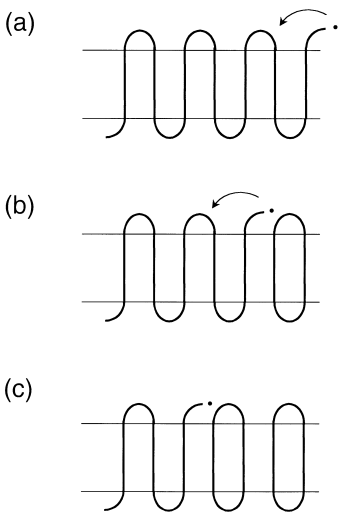

Fig. 3. Illustration of back-biting reaction scheme [54,55].

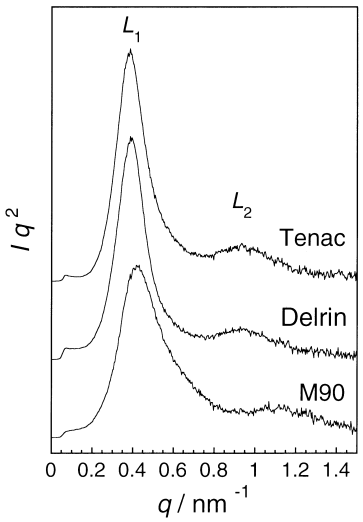

Fig. 4. Comparison of SAXS profile between Delrin, Tenac and M90 samples. The samples were prepared by melt and quenching into ice water bath.

SAXS L_2 peak. But the above-mentioned various experimental data cannot allow us to make such an interpretation any more. As already mentioned many times, the variation of relative intensity of L_1 and L_2 peaks depending on the sample preparation condition cannot support any such an idea of low-molecular-weight compounds included in the sample at a fixed content. Besides we do not know any reason why the L_2 peak of low-molecular-weight component shows almost the half value of the L_1 peak; the L_2 peak position may change depending on the molecular weight of this component. The observation of L_1 and L_2 peaks was reported for various kinds of polymers such as polyethylene [38–41], poly(ethylene terephthalate) [42], poly(aryletheretherketone) [43,44], etc. The ratio of long period L_1 and L_2 is almost 2 for all of these polymers. This ratio seems to be more than accidence and may be related to some non-accidental structure feature of stacked lamellae.

The next possibility is a lamella insertion model given in Fig. 1(c). The stacked lamellar structure of the L_1 long period is generated at first when the POM sample is cooled from the melt. At a lower temperature, the amorphous region sandwiched between the adjacent lamellae crystallizes to form a new lamella, giving a new SAXS peak with long period of $L_2 = L_1/2$. Ideally the ratio of L_1 and L_2 should be 2, but it is varied more or less depending on the structural regularity of lamella thickness and/or lamellar stacking period, as being explainable on the basis of Hosemann's second-kind of paracrystalline theory [28]. We need to consider how such a lamellar insertion model can be combined with the infrared spectroscopic data concerning the temperature dependence of FCC and ECC bands. Before doing so, we will analyze the SAXS data shown in Fig. 2 on the basis of a lamella insertion model [see Fig. 1(c)].

3.3. SAXS data analysis

The X-ray scattering intensity $I(q)$ was calculated for a lamella insertion model shown in Fig. 5. The scattering intensity was calculated using Eqs. (1) and (2).

$$I(q) = |F(q)|^2 \tag{1}$$

$$F(q) = \int_{-\infty}^{\infty} \rho(x) e^{-iqx} dx \tag{2}$$

where $F(q)$ is a structure factor and $\rho(x)$ is a one-dimensional electron density distribution along the lamellar stacking direction. The $\rho(x)$ is known when a concrete lamellar stacking model is given. For the lamella insertion model, we have various possible modifications. In model I in Fig. 5, new lamellae grow simultaneously at every position in between the already existing lamellae. In model II, the growing timing of lamella is different at each position and the density of lamella ($\Delta\rho$) has some distribution. In model III, the new lamella starts to appear from one end of already-existing lamellar stacking structure and the thus newly-built stacking structure evolves into the direction of other end side. In model IV the closely packed lamellar structure and the loosely packed lamellar structure are coexistent randomly. In all these models, the insertion of new lamellae is assumed to occur at 50% population. All of these models give essentially the same SAXS profiles as shown in Fig. 6. In other words, we cannot distinguish these models only from one SAXS profile. Therefore, as a model which can be treated most conveniently in the SAXS data analysis, we will employ here the model I. The growth of newly stacked lamellar structure is expressed as an increment of electron density of these lamellae. In fact, as shown in Fig. 7, the SAXS profile is calculated to change from the pattern with high peak at L_1 position to the pattern with high peak at L_2 position [see Fig. 7(b)] when the electron density of new lamellae Δ_2 is changed from 0 to 1 [see Fig. 7(a)].

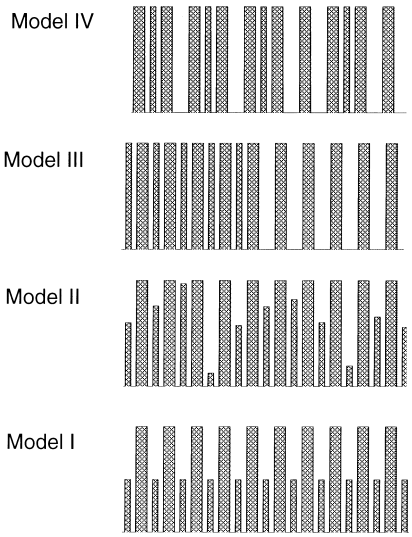

Fig. 5. Various types of lamella insertion model. Model I: inserted lamellae grow simultaneously at all the positions. Model II: growing timing of inserted lamellae is random. Model III: inserted lamella starts to appear from one end and evolves in the direction of other end. And Model IV: inserted lamellae exist in random fashion. (It is noted here that the lamellae in the actual sample may be packed in a disordered manner as for the repeating period and the size of repetition.)

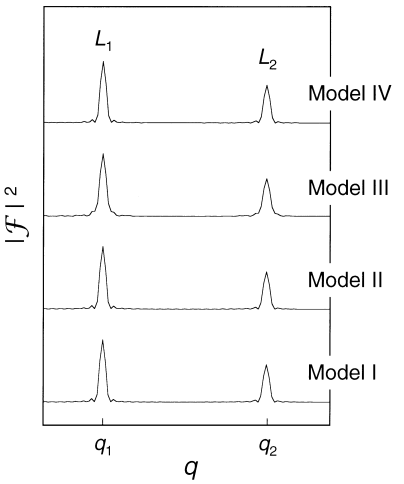

Fig. 6. Scattering intensities calculated for the models shown in Fig. 5.

The SAXS data analysis was made by a curve fitting method, where the various parameters necessary for description of stacked lamellar structure were determined so that the calculated scattering profile was as closely fitted to the observed data as possible. The parameters to be determined are shown in Fig. 8. The lamellae were assumed to have the sharp edges and the electron density distribution of square shape. The electron density of lamellae with long period L_1 is Δ_1 and that of lamellae with long period L_2 is Δ_2. The total number of original lamellae is N. In the calculation this N was set to infinite and the stacking disorder was introduced to the regular model, i.e. Hosemann's second-kind of paracrystalline theory [28]. The long

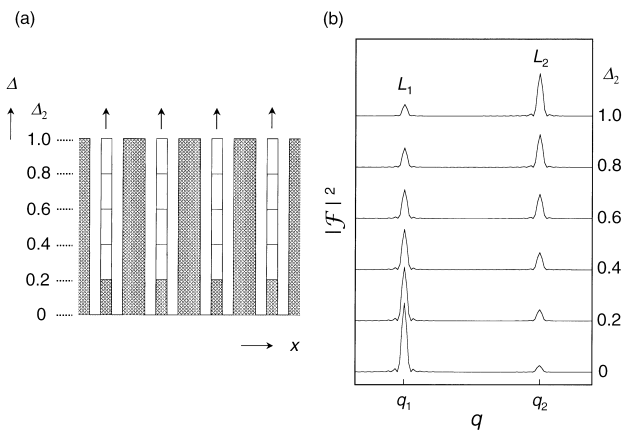

Fig. 7. Insertion structures. (a) Insertion of new lamellae between the originally-existing lamellae, and (b) the corresponding SAXS profile change calculated by changing the electron density Δ_2.

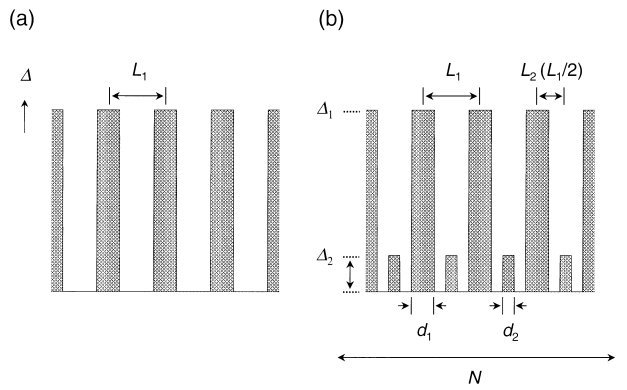

Fig. 8. Two types of lamellar stacking structure. (a) Two phase model and (b) inserted lamellar stacking structure. L_1 is the long period between main lamellae, L_2 is the half value of long period of L_1, Δ_1 is the relative electron density of main lamellae, Δ_2 is the relative electron density of inserted lamellae, d_1 is the crystal thickness of main lamellae, d_2 is the crystal thickness of inserted lamellae, and N is the number of stacked lamellae.

period L_1 (and L_2) was assumed to distribute at a Gaussain distribution probability, meaning that the lamellae form a kind of finite domain substantially and the whole size of the domain was finite. The scattering intensity $I(q)$ is expressed by Eq. (3) [29].

$$I(q) = P(q)L(q) \tag{3}$$

where $P(q)$ is a particle factor and $L(q)$ is a lattice factor. $P(q)$ is a square of Fourier-transformation of structure unit. $L(q)$ is a square of Fourier-transformation of 1-dimensional periodicity with second-kind of disorder. As a trial we calculated the SAXS profile by using a model (a) in Fig. 8, i.e. a 2-phase model consisting of an alternate repetition of crystalline and amorphous phases. In this case, the particle factor $P(q)$ is given by Eqs. (4) and (5). The lattice factor $L(q)$ is given by Eq. (6) [28]. As a result the scattering intensity is given by Eq. (7).

$$\rho(x) = \begin{cases} \Delta(-d/2 \le x \le d/2) \\ 0(x < -d/2, d/2 < x) \end{cases} \tag{4}$$

$$P(q) = \left|\int_{-\infty}^{\infty} \rho(x)\mathrm{e}^{-iqx}\mathrm{d}x\right|^2 = \left(\int_{-d/2}^{d/2} \Delta\cos(qx)\mathrm{d}x\right)^2 = \frac{4\Delta^2\sin^2(\mathrm{d}q/2)}{q^2} \tag{5}$$

$$L(q) = \frac{1-\exp(-4\pi^2g^2h^2)}{[1-\exp(-2\pi^2g^2h^2)]^2 + 4\sin^2(\pi h)\exp(-2\pi^2g^2h^2)} = \frac{\sinh(q^2\sigma_L^2/2)}{\cosh(q^2\sigma_L^2/2) - \cos(Lq)} \tag{6}$$

$$I(q) = \frac{4\Delta^2\sin^2(\mathrm{d}q/2)}{q^2}\frac{\sinh(q^2\sigma_L^2/2)}{\cosh(q^2\sigma_L^2/2) - \cos(Lq)} \tag{7}$$

where Δ is the difference of electron density between crystalline and amorphous phases, d is the thickness of a lamella, L is the lamellar periodicity or long period, g is the Hosemann's g factor and is defined as $g = \sigma_L/L$, and h is defined as $h = Lq/2\pi$. σ_L is the standard error of Gaussian distribution for L. When this function was applied to the SAXS data observed at room temperature, we could not reproduce the whole SAXS profile even when the parameters were varied in any way [see Fig. 9].

Thus, as mentioned above, we will apply now the lamella insertion model. In this case the $P(q)$ and $L(q)$ are given by the following equations.

$$\begin{aligned} P(q) &= \left|\int_{-\infty}^{\infty} \rho(x)\mathrm{e}^{-iqx}\mathrm{d}x\right|^2 \\ &= \left|\frac{2\Delta_1\sin(d_1q/2)}{q} + \frac{2\Delta_2\sin(d_2q/2)}{q}\exp(-iLq/2)\right|^2 \\ &= 4[\Delta_1^2\sin^2(d_1q/2) + 2\Delta_1\Delta_2\cos(Lq/2)\sin(d_1q/2) \\ &\quad \times\sin(d_2q/2) + \Delta_2^2\sin^2(d_2q/2)]/q^2 \end{aligned} \tag{8}$$

$$L(q) = \frac{1-\exp(-4\pi^2g^2h^2)}{[1-\exp(-2\pi^2g^2h^2)]^2 + 4\sin^2(\pi h)\exp(-2\pi^2g^2h^2)} = \frac{\sinh(q^2\sigma_L^2/2)}{\cosh(q^2\sigma_L^2/2) - \cos(Lq)} \tag{9}$$

As a result, the scattering intensity $I(q)$ is given by Eq. (10).

$$I(q) = \frac{4[\Delta_1^2\sin^2(d_1q/2) + 2\Delta_1\Delta_2\cos(Lq/2)\sin(d_1q/2)\sin(d_2q/2) + \Delta_2^2\sin^2(d_2q/2)]\sinh(q^2\sigma_L^2/2)}{q^2[\cosh(q^2\sigma_L^2/2) - \cos(Lq)]} \tag{10}$$

where Δ_1 is the difference of electron density between the main crystalline phase and amorphous phase, Δ_2 is the difference of electron density between the amorphous phase and the inserted lamella, which is sandwiched between the main lamellae, d_1 is the thickness of a main lamella, d_2 is the thickness of inserted lamella, and L is the lamellar periodicity or long period. It was assumed that an inserted lamella exists at the intermediate position of the two neighboring original lamellae. These parameters were determined by carrying out the least-squares curve fitting

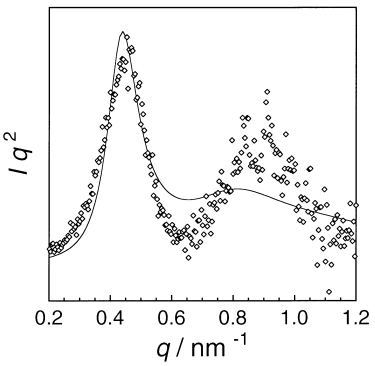

Fig. 9. Curve-fitting result obtained for the 2-component model [see Fig. 8(a)]. The open circle is the experimental data and the solid line is a calculated curve.

for the observed SAXS profile. One example of curve fitting is shown in Fig. 10(a) in comparison with the observed SAXS profile. The corresponding model is shown in Fig. 10(b).

3.4. Temperature dependence of stacked lamellar structure parameters

Fig. 11 shows the temperature dependence of the thus estimated structural parameters in the cooling process from the melt. When the POM sample was cooled from the melt, the main lamellae started to appear with the long period of ca. 17 nm. The thickness (d_1) of these lamellae is about 4 nm. The g factor as a measure of lamellar stacking disorder is ca. 0.26 around the crystallization temperature. As the temperature was decreased, the difference of electron density between crystalline and amorphous phase (Δ_1) and the lamellar thickness (d_1) grew up. On the other hand, the long period L and the g factor decreased steeply. This indicates that the lamellar stacking became tight in good order. Around 140 °C, the thickness of main lamella (d_1) is 6.5 nm and the long period reaches 15 nm, and the new thin lamellae started to appear between main lamellae. The electron density difference Δ_2 increased gradually with

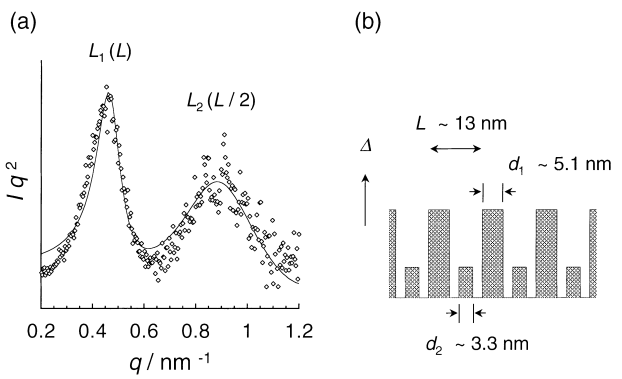

Fig. 10. An example of curve fitting result obtained for the lamella insertion model [Fig. 8(b)]. (a) A comparison between the observed SAXS profile (open circle) and the theoretical scattering curve (solid line) and (b) the thus obtained lamellar structure.

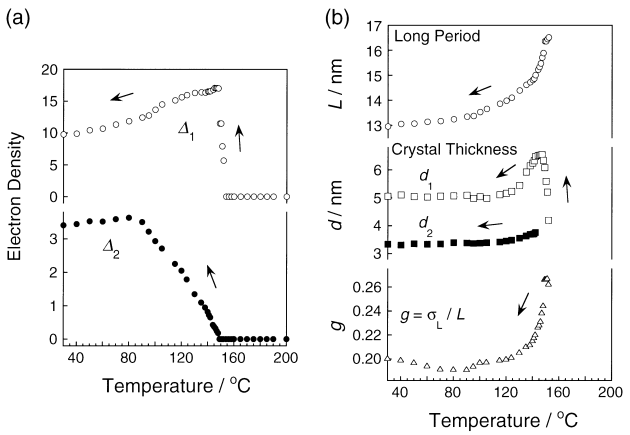

Fig. 11. Temperature dependence of the structure parameters obtained for the lamella insertion model. (a) Temperature dependence of Δ_1 and Δ_2, and (b) temperature dependence of long period, crystal thickness and g parameter.

decreasing temperature. The inserted lamellar thickness (d_2) was almost constant. As the temperature was cooled down to about 100 °C, the structure was almost stabilized. The structural change of stacked lamellae is illustrated in Fig. 12. In Figs. 12(b) and 13, more realistic lamellar stacking structure is shown by taking the statistical distribution of original and newly-generated lamellae into consideration as discussed in Fig. 5. As the temperature decreased, the number of inserted lamellae increased and the amorphous region was filled by these lamellae. (It should be noticed here that the lamellae in the models shown in Fig. 13 are stacked regularly along the x-axis, but these lamellae are considered to be arrayed in a disordered manner in the actual sample as known from the introduction of Gaussian-type stacking fault.).

3.5. Combination of IR, SAXS and WAXS data

Fig. 14 shows the temperature dependence of WAXS

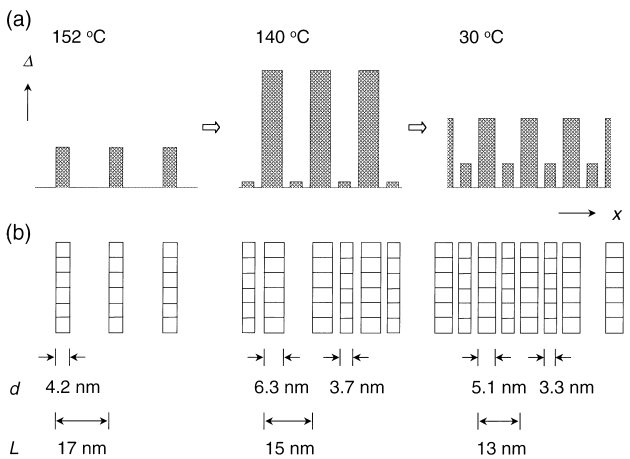

Fig. 12. Temperature dependence of lamella insertion model in cooling process of POM from the melt. (a) Temperature dependence of 1-demensional electron density profile, and (b) more realistic lamellar stacking model.

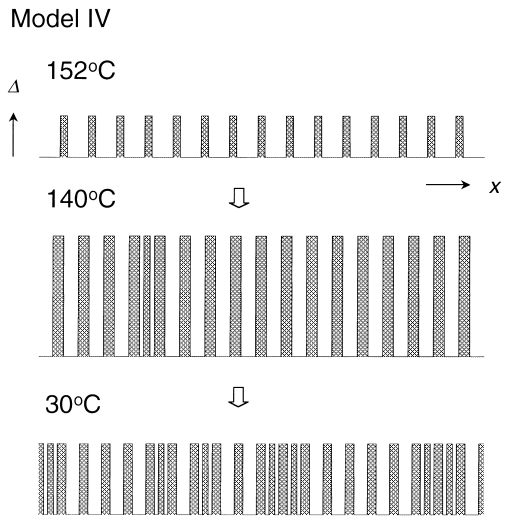

Fig. 13. Temperature dependence of stacked lamellar structure in the cooling process of POM from the melt. (It is noted here that the lamellae in the actual sample may be packed in a disordered manner as for the repeating period and the size of repetition, as discussed in the text.)

profile measured in the cooling process from the melt. The *a*-axial length was evaluated from the (100) reflection position and the peak position of the amorphous halo was also read out to know the change in the amorphous structure. Fig. 15 shows the comparison of various experimental data of SAXS, WAXS and IR. As pointed out in the previous paper [50], the infrared spectral measurement gave information on the generation of FCC and ECC morphologies in the temperature region where the SAXS L_1 and L_2 peaks appeared, respectively. From the discussion made there, the detected ECC morphology does not necessarily mean the real extended chain crystallites but may be a unit having similar structural characteristics to those of ECC. If this unit is assumed as a cylinder constructed by aggregated chains, the ratio of height and radius of the cylinder is about 0.1–0.2 judging from the wavenumber of the infrared ECC band [51]. As one possibility we draw the 'ECC-like' structural unit as shown in Fig. 16, which may be called the

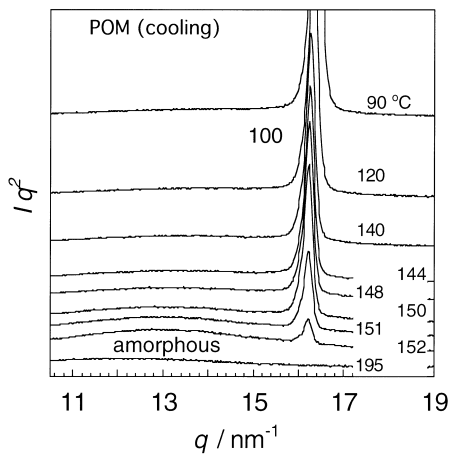

Fig. 14. Temperature dependence of WAXS profile measured in the cooling process of POM from the melt.

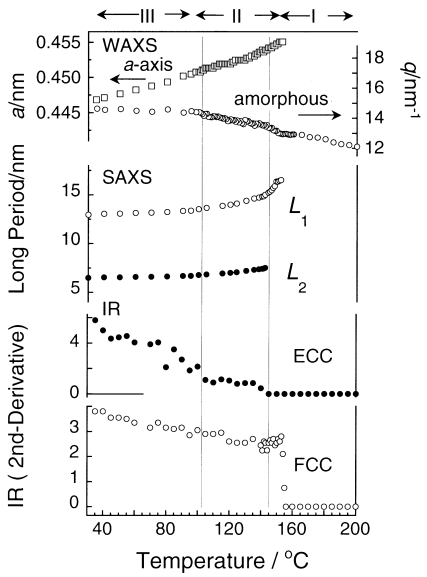

Fig. 15. Temperature dependence of the *a*-axis length of the unit cell, the peak position of the amorphous halo, the long periods of SAXS L_1 and L_2 peaks, and the infrared intensities of ECC and FCC bands.

taut tie molecules passing through the neighboring lamellae. By combining the thus collected all information concerning the chain aggregation, morphology, stacked lamellae and so on [see Fig. 15], we may draw the structural evolution in the cooling process from the melt as shown in Fig. 16.

Temperature region I. In the vicinity of crystallization temperature, FCC band started to appear and grew steeply. The molecular chains were regularized to give lamellae, reflecting on the SAXS L_1 peak with ca. 17 nm long period. The amorphous halo shifted to higher q side with decreasing temperature and held the position during an occurrence of the crystallization (~160 °C) and then again shifted. The *a*-axial length became shorter, indicating a closer chain packing in the crystal lattice. It may be speculated that the amorphous region is contracted more or less in the cooling process from the melt and some nuclei are generated from the parts of higher density in the amorphous region. As the temperature decreases furthermore, the crystalline density is increased gradually as known from the change in the *a*-axial length.

Temperature region II. With decreasing in temperature, around 140 °C, ECC band started to appear in the infrared spectra and grew gradually. The SAXS L_2 peak appeared at ca. 7 nm. A new thin lamella was inserted in between the

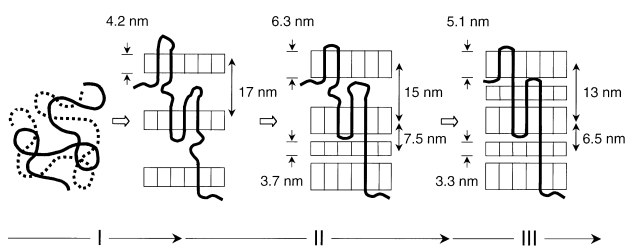

Fig. 16. An illustration of structural evolution in the crystallization process of POM from the melt.

main lamellae, giving the L_2 peak with almost the half long period and resulting also in the formation of taut tie molecules passing through these lamellae.

Temperature region III. As the temperature approaching the room temperature, FCC band intensity was almost saturated, but the ECC band increased the intensity furthermore. It is speculated that the number of the taut tie molecules still increases in this temperature region.

4. Conclusions

In the present paper, the structural change in the non-isothermal crystallization process of POM cooled from the molten state was investigated by the SAXS and WAXS measurements as functions of temperature. The data analysis gave us a reasonable model concerning the evolution procedure of lamellar stacking structure. This information was combined together with the previously reported infrared spectral data, from which the structural changes occurring in the crystallization process was extracted concretely from the molecular level.

When the POM sample was cooled slowly from the melt, the SAXS peak corresponding to the stacked lamellar structure with the long period of ca. 14 nm (L_1) was found to grow. At the same time, the infrared bands characteristic of folded chain crystal (FCC) morphology were detected. At around 140 °C, a new peak of long period of ca. 7 nm (L_2) was found to appear and increased in intensity. The peak height of L_1 decreased in parallel. In the same temperature region the infrared bands intrinsic of extended chain crystal (ECC) morphology were detected to increase in intensity. The intensity exchange of the SAXS L_1 and L_2 peaks has been interpreted reasonably on the basis of a lamella insertion model. That is, the stacked lamellar structure of FCC morphology appeared around 156 °C with a long period of 14 nm and the amorphous region sandwiched between the neighboring two lamellae changed to a new lamella around 140 °C and as a result the long period was reduced to 7 nm, a half value of 14 nm.

In the actual sample, the lamellar stacking structures of long periods L_1 and L_2 are considered to coexist randomly along the normal to the lamellar surface to exhibit the two SAXS peaks. Some of the chains pass through the several neighboring lamellae and form apparently the taut tie chains as an ECC-like structure.

In order to clarify the structural evolution process in more detail, we need to carry out the isothermal crystallization experiment and to measure the IR, SAXS and WAXS as a function of time at the various constant temperatures. The detailed analysis will be reported in a near future.

Acknowledgements

The authors wish to thank Polyplastics Co. Ltd., Japan for kindly supplying POM sample. They also thank Dr Masatoshi Iguchi (Research Institute for Polymers and Textiles, Tsukuba, Japan) for kindly supplying POM whisker.

References

[1] Geil PH. J Polym Sci 1960;47:65.
[2] Geil PH. J Polym Sci Part C 1966;13:149.
[3] Burmester A, Geil PH. In: Pae RD, Morrow DR, Chen Y, editors. Advances in polymer science and engineering. New York: Plenum Press; 1972. p. 42–100.
[4] Mihailov M, Terlemezyan L. Dokl Bolg Akad Nauk 1975;28:643.
[5] Salaris F, Turturro A, Bianchi U, Martuscelli E. Polymer 1978;19: 1163.
[6] Terlemezyan L, Mihailov M, Schmidt P, Schneider B. Makromol Chem 1978;179:807.
[7] Terlemezyan L, Mihailov M, Schmidt P, Schneider B. Makromol Chem 1978;179:2315.
[8] Terlemezyan L, Mihailov M. Makromol Chem 1978;179:2807.
[9] Cutler DJ, Hendra PJ, Scerri ER, Cudby MEA, Willis HA. Polymer 1979;20:1470.
[10] Schmidt P, Schneider B, Baldrian J, Terlemezyan L, Mihailov M, Ivanova B. Polymer 1987;28:217.
[11] Franbourg A, Rietsch F. Polym Bull 1990;24:445.
[12] Martin JA, Cruz-Pinto JJC. J Therm Anal 1993;40:621.
[13] Martin JA, Cruz-Pinto JJC, Oliveira MJ. J Therm Anal 1993;40:629.
[14] Cruz-Pinto JJC, Martins JA, Oliveira MJ. Colloid Polym Sci 1994; 272:1.
[15] Plummer CJG, Kausch H-H. Polym Bull (Berlin) 1994;32:117.
[16] Plummer CJG, Kausch H-H. Colloid Polym Sci 1995;273:227.
[17] Plummer CJG, Kausch H-H. Colloid Polym Sci 1995;273:719.
[18] Plummer CJG, Menu P, Cudre-Mauroux N, Kausch H-H. J Appl Polym Sci 1995;55:489.
[19] Phillips R, Manson J-AE. J Polym Sci Polym Phys 1997;B35:875.
[20] Yeh F, Hsiao BS, Chu B, Sauer BB, Flexman EA. J Polym Sci 1999; B37:3115.
[21] Sauer BB, Hsiao BS, Wang Z-G. Polym Mater Sci Engng 1999;81: 361.
[22] Geil PH. Polymer 2000;41:8983.
[23] Sauer BB, Mclean RS, Londono JD, Hsiao BS. J Macromol Sci Phys 2000;B39:519.
[24] Samon JM, Schultz JM, Hsiao BS, Khot S, Johnson HR. Polymer 2000;42:1547.
[25] Samon JM, Schulz JM, Hsiao BS. Polymer 2002;43:1873.
[26] Martins JA, Cruz Pinto JJC. Polymer 2002;43:3999.
[27] Hermans JJ. Recueil Trav Chim Pays-Bas 1944;63:5.
[28] Hosemann R, Bagchi SN. Direct Analysis of Diffraction by Matter. Amsterdam: North-Holland; 1962. p. 410.
[29] Reinfold C, Fischer EW, Peterlin A. J Appl Phys 1964;35:71.
[30] Tsvankin DY. Polym Sci USSR 1964;6:2304.
[31] Blundell DJ. Acta Crystallog 1970;A26:472.
[32] Buchnan DR. J Polym Sci A-2 1971;9:645.
[33] Crist B. J Polym Sci, Polym Phys 1973;11:635.
[34] Bonart R, Muller EH. J Macromol Sci, Phys 1974;B10:177.
[35] Beumer H, Hosemann R. J Macromol Sci, Phys 1978;B15:1.
[36] Hosemann R, Hindelch AM. J Macromol Sci, Phys 1995;B34:327.
[37] Crist B. J Macromol Sci, Phys 2000;B39:493.
[38] Geil PH. Bull Am Phys Soc 1962;7:206.
[39] Hoffman JD, Weeks JJ. J Chem Phys 1965;42:4301.
[40] Sasaki S, Tashiro K, Kobayashi M, Izumi Y, Kobayashi K. Polymer 1999;40:7125.
[41] Akpalu YA, Amis EJ. J Chem Phys 2000;113:392.
[42] Lee CH, Saito H, Inoue T, Nojima S. Macromolecules 1996;29:7034.
[43] Hsiao BS, Gardner KH, Wu DQ, Chu B. Polymer 1993;34:3986.

[44] Hsiao BS, Gardner KH, Wu DQ, Chu B. Polymer 1993;34:3996.
[45] Song HH, Stein RS, Wu DQ, Ree M, Phillips JC, LeGrand A, Chu B. J Polym Sci, Polym Phys B 1988;21:1180.
[46] Song HH, Wu DQ, Chu B, Satkowski M, Ree M, Stein RS, Phillips JC. Macromolecules 1990;23:2380.
[47] Li Y, Jungnickel B-J. Polymer 1993;34:9.
[48] Dreezen G, Mischenko N, Koch MHJ, Reynaers H. Groeninckx Macromol 1999;32:4015.
[49] Yeh F, Hsiao BS, Chu B, Sauer BB, Flexman EA. J Polym Sci, Polym Phys B 1999;37:3115.
[50] Hama H, Tashiro K. Polymer, in press.
[51] Kobayashi M, Sakashita M. J Chem Phys 1992;96:748.
[52] Tadokoro H, Yasumoto T, Murahashi S, Nitta I. J Polym Sci 1960;44: 266.
[53] Uchida T, Tadokoro H. J Polym Sci A-2 1967;5:63.
[54] Hasegawa M, Yamamoto K, Shiwaku T, Hashimoto T. Macromolecules 1990;23:2629.
[55] Lucke A. Doctoral Thesis, Freiburg University, 1979.